PHILOSOPHICAL TRANSACTIONS OF THE ROYAL SOCIETY A MATHEMATICAL, PHYSICAL & ENGINEERING SCIENCES

A modified split Hopkinson torsional bar system for correlated study of τ–γ relations, shear localization and microstructural evolution

Rong Yang, Husheng Zhang, Letian Shen, Yongbo Xu, Yilong Bai and Bradley Dodd

Phil. Trans. R. Soc. A 2014 **372**, 20130208, published 7 April 2014

PHILOSOPHICAL TRANSACTIONS OF THE ROYAL SOCIETY A

rsta.royalsocietypublishing.org

Research

Cite this article: Yang R, Zhang H, Shen L, Xu Y, Bai Y, Dodd B. 2014 A modified split Hopkinson torsional bar system for correlated study of $\tau-\gamma$ relations, shear localization and microstructural evolution. *Phil. Trans. R. Soc. A* **372**: 20130208.
http://dx.doi.org/10.1098/rsta.2013.0208

One contribution of 12 to a Theme Issue 'Shock and blast: celebrating the centenary of Bertram Hopkinson's seminal paper of 1914 (Part 1)'.

Subject Areas:
mechanics

Keywords:
modified split Hopkinson torsional bars, shear localization, microstructural evolution

Author for correspondence:
Rong Yang
e-mail: yangr@lnm.imech.ac.cn

A modified split Hopkinson torsional bar system for correlated study of $\tau-\gamma$ relations, shear localization and microstructural evolution

Rong Yang[1], Husheng Zhang[1], Letian Shen[1], Yongbo Xu[2], Yilong Bai[1] and Bradley Dodd[3]

[1]The State Key Laboratory of Nonlinear Mechanics, Institute of Mechanics, Chinese Academy of Sciences, Beijing 100190, People's Republic of China
[2]Shenyang National Laboratory for Materials Science, Institute of Metal Research, Chinese Academy of Sciences, Shenyang 110016, People's Republic of China
[3]Institute of Shock Physics, Imperial College London, London SW7 2AZ, UK

The conventional split Hopkinson torsional bar (SHTB) system consists of two bars, which can successfully produce the data for the construction of dynamic torsional shear stress and strain relationships. However, the system cannot provide reliable information on the progression of the deformed microstructure during the test. The reverberation of waves in the bars and the tested specimen can spoil the microstructural pattern formed during the effective loading. This paper briefly reviews a modified version of the SHTB system consisting of four bars that has been developed. This modified system can eliminate the reverberation of waves in the specimen and provide only a single rectangular torsional stress pulse, thus it can properly freeze the microstructure formed during the effective period of loading in the specimen. By using the advantage of the modified SHTB system, together with a new design of specimen, it is possible to perform a correlated study of the dynamic stress–strain response, shear localization and the evolution of

Royal Society Publishing

the microstructure at a fixed view-field (position) on a given specimen during the sequence of the loading time. The principles, experimental set-up and procedure, calibration and some preliminary results of the correlated study are reported in this paper.

1. Introduction

It has been a century since the Hopkinson pressure bar was introduced by Bertram Hopkinson in 1914 [1] as a way to measure elastic wave propagation in a metal bar. Later, Kolsky [2] refined this technique to measure stress and strain, by using two Hopkinson bars in series, which is now known as the split Hopkinson pressure bar (SHPB). SHPBs have been widely used since the 1970s and increasingly have become the standard method of measuring material dynamic mechanical properties in compression in the strain rate range of 10^3–$10^4\ s^{-1}$, and then tension and torsion [3,4] versions were developed [5].

The conventional Hopkinson bar system uses two bars, which can be used to obtain the dynamic constitutive stress–strain relationships of materials, but it cannot freeze the deformed microstructure at a certain plastic deformation owing to the reverberation waves in the system. By using stress-reversal momentum trapping techniques, Nemat-Nasser *et al.* [6] were the first to perform single-pulse loading using a tensile bar system; however, an interrupted torsion loading was difficult to achieve. Our apparatus was a four-bar torsion system, which was modified using an unloading bar and a specially designed clutch to suppress reflected waves [7,8], so that the effect of loading reverberation was eliminated, and a correlation of evolving microstructures with the transient shear stress–strain recording was made possible. Based on post-mortem observations, the previous work of Bai, Xue, Xu and co-workers [7–11] on the evolution of shear localization using this apparatus had investigated the relationship between the deformed microstructure and the macroscopic stress–strain response. However, those results were based on a series of identical specimens, which were tested to different degrees of plastic deformation. The macroscopic stress–strain response of the materials was not well correlated with the microstructure evolution of each specimen, owing to variations in microstructure as well as dynamic response in those 'identical' specimens. This is the problem we attempt to solve in this paper.

Shear localization in a material is abrupt and uncontrollable and usually leads to dramatic structural consequences, thus a lot of attention has been focused on this field. Much work in the theoretical analysis and numerical simulations has been performed, to predict the process of shear localization, and to determine the factors governing the process [12–16]. Comparisons of the theory of the scaling laws [17–19] and experiments on the process of shear localization have been made, by using an infrared technique to measure the temperature distribution [20] and history [13,21] of shear localization, and by means of high-speed photography and a grid pattern to observe the transient deformation field in the process of shear localization [20,22]. The physical mechanism of this phenomenon has usually been treated as a thermo-mechanical instability, driven by the high strain rate softening effect. However, there has been debate on possible alternative material softening mechanisms, such as dynamic recrystallization (DRX) by Rittel *et al*. [23]. They found that the temperature rise prior to localization was quite modest [24,25], and DRX was observed to be the only mechanism of failure in pure Ti specimens by scanning electron microscope examination. To find out what occurs during shear localization is a further driving force for this work.

This paper reports the experimental results of the evolution of the microstructure in aluminium alloy 2024 and Ti6A14V alloy; the latter material is known to be very sensitive to shear banding. A series of tests have been carried out on each specimen with the modified split Hopkinson torsional bar (SHTB) to investigate the evolving microstructure in shear localization at an approximate strain rate of $10^3\ s^{-1}$. In order to coordinate the evolving microstructure with the

macroscopic stress–strain response, modifications were made in this work: (i) the shape of the specimen was redesigned so that the deformed surface and microstructure could be observed with the sample *in situ*; (ii) fixed view-field deformations of the sample were captured by a camera after each pulse loading, and then analysed by a digital image correlation (DIC) algorithm to obtain the deformation and strain field; and (iii) some preliminary tests were performed, and the microscopic characteristics in the localization process corresponding to the transient τ–γ curves were correlated and analysed. By using this system, the shear band formation and accompanying phenomena can be investigated, from which it is possible to reveal what occurs during the shear localization process.

2. Experiments

(a) Test system

The SHTB apparatus consists of four bars, one dynamic strain recording set and a camera pack. All six parts are shown in figure 1. In the middle, the apparatus is the same as a conventional SHTB system: the incident bar has strain gauges attached and a high-speed amplifier, the specimen and the transmission bar are attached to another amplifier. In order to eliminate the reverberation of torsion waves owing to wave reflection at the bar ends, one unloading bar with a specially designed clutch was connected to the incident bar, and another unloading bar with the same connector was installed at the end of the transmission bar. The two above-mentioned clutches separate from the bars in the middle automatically after the loading pulse has passed through the specimen completely. In this manner, most of the reflected waves from both ends were transmitted out of the loading system after the first loading, and the residual secondary waves were considerably smaller, thus no plastic deformation was imposed on the specimen after the effective torsion wave pulse.

The clamp can be moved along the rails to adjust the loading pulse duration; also the strain applied to the strain gauge can be modified so that different torsion momentum and strain rate can be achieved, which made the controllable interrupting tests possible.

The amplifier signal was monitored by an oscilloscope and then recorded by a computer; meanwhile, a camera system was set up to take pictures of the thin wall of the specimen. The surface of the sample was marked with ink or lines, so that the macro-deformation and the microstructural evolution after each loading of the same region could be tracked and recorded accurately.

(b) Test materials and specimen

Two kinds of materials were chosen to be tested. The chemical compositions are shown in table 1. The shape of the specimen was modified to facilitate macro-deformation and microstructure observation, as shown in figure 2. The gauge length was increased to 3.5 mm for polishing and microstructural etching, so that *in situ* observation after each test was possible; wrinkles would emerge if the gauge length was increased to 5 mm owing to buckling of the thin wall under torsional loading. The internal diameter was made larger to facilitate the observation. However, the thickness of the specimen was reduced, so that the torsional momentum generated from the test instrument was enough to deform the specimen. The ends of the specimen were connected to screw threads, one was glued and installed on the transmission bar, and the other was fastened by a wrench to the incident bar.

(c) Procedure

The apparatus was first calibrated using a dummy sample to guarantee the accuracy of the relationship between the loading torque and the strain voltage, the duration of the pulse and the elimination of the loading reverberation. Then the specimen was installed, with the movable

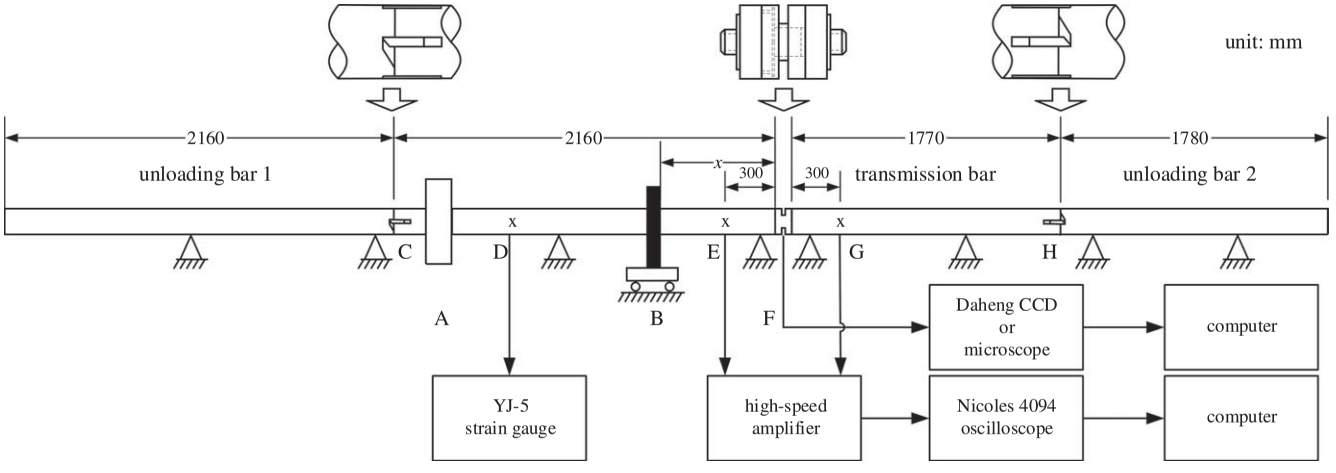

Figure 1. Schematic of the test system. A, loading end; B, movable clamp; C and H, connector; D, E and G, strain rosettes; F, specimen and camera.

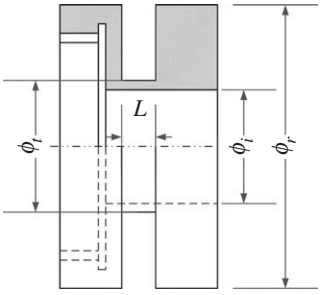

Figure 2. Modified sample shape.

Table 1. Chemical composition of the AA2024 and Ti6Al4V alloy (mass fraction %).

materials	alloying element									
AA2024	Al	Cu	Mg	Mn	Fe	Si	Zn	Ni	Ti	rest
	rest	3.8–4.9	1.2–1.8	0.3–0.9	0.5	0.5	0.3	0.1	0.15	0.15
Ti6Al4V	Al	V	Ti	Fe	Si	C	N	H	O	rest
	5.5–6.8	3.5–4.5	rest	0.30	0.15	0.10	0.05	0.015	0.20	0.40

clamp locked. The junctions with the screw were tightened to remove the clearance so that the torque pulse could pass through without any loss. The outsides of the specimen and connector were marked to see whether permanent deformation occurred to the specimen and whether the links were firmly fastened.

After the specimen was installed, the camera was mounted, and pictures of the undeformed specimen were recorded followed by a process of calibrating the image pixel to actual length. After that, the incident bar was loaded, and then the clamp was released, the torque momentum travelled in the bar system and finished loading and unloading of the specimen. After each interrupting test, the bars were rotated to their original positions, and the post macro-deformation and microstructure were captured. Then the clamp was locked, and loaded again until the specimen failed.

3. Experimental observations and results

A series of tests were performed on the modified SHTB, and the averaged strain rate was about $2 \times 10^2\,\mathrm{s}^{-1}$. The specimens had different gauge lengths and thicknesses; the detailed shape and test parameters can be found in figure 2 and table 2.

Figure 3 shows the typical input and transmitted pulse signals of the AA2024 (specimen A8 for the first loading) and Ti6Al4V tests; the secondary and subsequent pulses were successfully suppressed. However, after the separation of the unloading bars, the reflected waves were trapped in the incident bar and transmission bar and attenuated gradually.

(a) AA2024

AA2024 specimens with different thickness and gauge length were tested. The specimens with a 2 mm test region were hard to polish, thus they were used to correlate the stress–strain relationship with the macro-deformation. The ones with a 3.5 mm gap were polished and etched, to observe the microstructural evolution after each pulse loading. Some of the specimens fractured during the first loading. After fracture, the surfaces were damaged, and the previous positions of

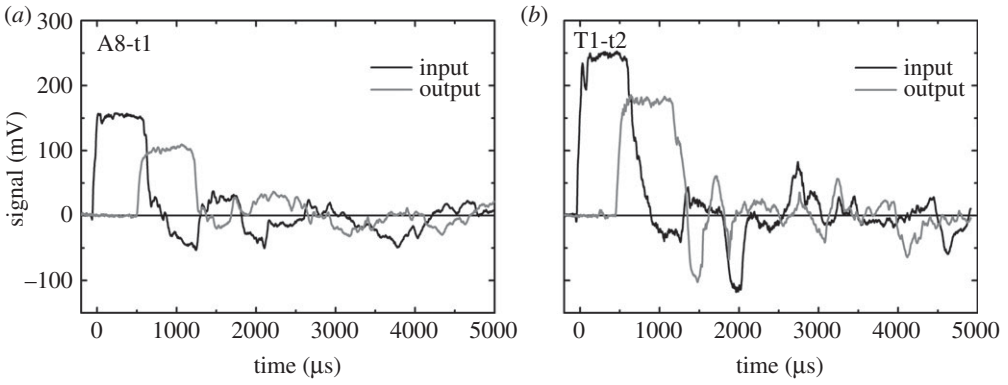

Figure 3. Input and transmitted pulse signals. (*a*) AA2024 and (*b*) Ti6Al4V.

Table 2. Shape and loading parameters.

specimen	ϕ_i (mm)	ϕ_t (mm)	L (mm)	thickness (mm)	duration (μs)	loading rate (s^{-1})	failure mode
A8	15.90	16.68	1.95	0.39	600	100–200	fracture, seven tests
A17	16.49	15.99	3.50	0.25	600	90–300	fracture, one test
A18	16.50	16.02	3.50	0.26	600	90–300	fracture, one test
A19	16.49	16.00	3.50	0.255	600	90–300	fracture, 10 tests
T1	15.88	16.46	3.45	0.29	800	100–200	fracture, seven tests
T3	16.32	16.00	3.50	0.16	n.a.	n.a.	buckling, one test
T4	15.32	16.00	3.50	0.16	600	100–300	fracture, four tests

the undeformed images were impossible to locate. However, some specimens endured, two of which are described below.

Figure 4*a–h* shows stress–strain curves for A8, together with the correlated pictures of macro-deformation and the DIC analysis results of shear strain. The magnification of the optical system was set to be low so that the whole length of the tested section (2 mm) could be observed in one picture. It survived five rectangular torsional pulses and fractured on the sixth. All six stress–strain curves were aligned into one curve, as shown in figure 4*a*. It was found that, during the sixth loading, the stress–strain dropped, and a crack was observed in the specimen along the circular direction.

The shear strains from the strain gauge measurements, as well as those from DIC calculations, are shown in table 3 and figure 4. For the DIC analysis, the image size is 2048 × 1536 pixels, and the specimen lies in a 1600 × 1536 pixel area (200 pixels to the left of the image). The DIC analysis shows that the shear strain distribution was not uniform along the z-direction, while it remained constant in the circular direction. Deformation localization occurred in the middle of the section, where shear strain was higher since the first loading and remained that way until the specimen fractured.

Figure 5 shows the results of specimen A19. Its surface was polished and etched, and metallurgical information could be retrieved from the picture. The grain boundaries were shattered during the production process; they are shown as the black dots distributed horizontally in figure 5*a*. The thick lines along the vertical direction are the remaining traces of machining after the polishing process.

Shear localization was also observed in A19 after the ninth loading, and the deformation was quite uniform during the previous eight tests. After each test, wrinkles could be observed on

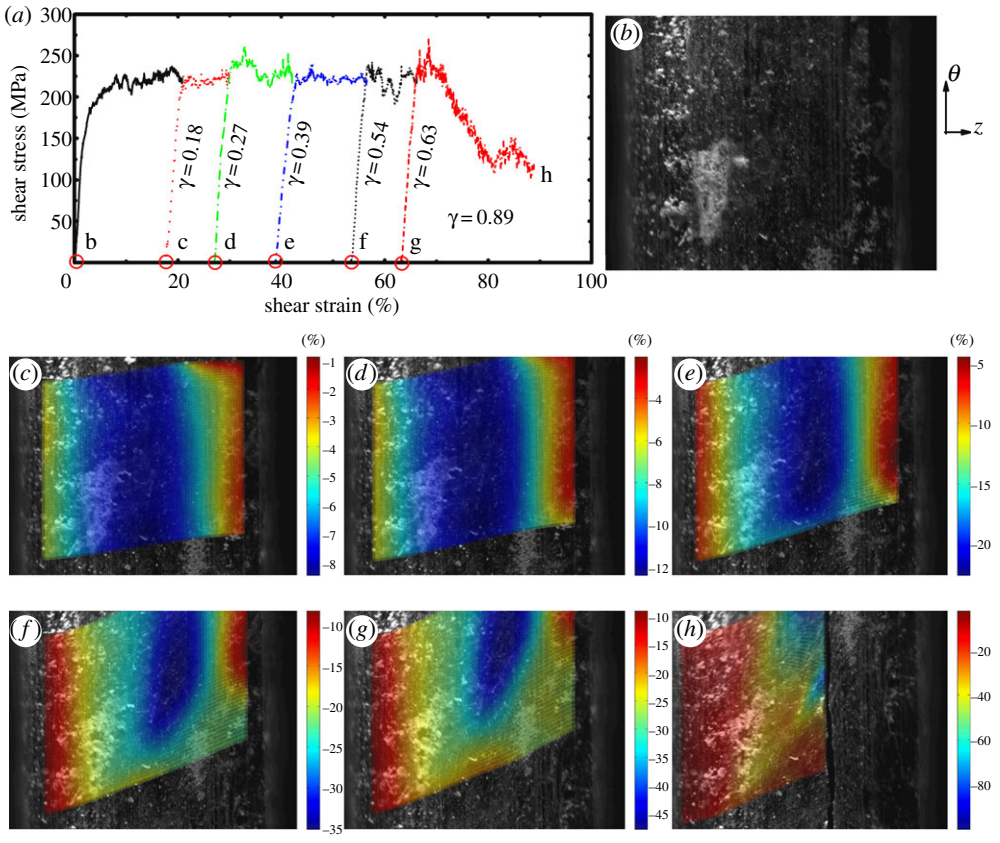

Figure 4. Strain and stress curves and correlated deformation analysis of each frozen test for AA2024 specimen A8. The shear strain is plotted on the deformed configuration. The shear localization occurred in the middle of the sample, where cracking emerged after six tests. (*a*) The strain and stress curves; (*b*) undeformed surfaces; (*c–h*) shear strain distribution after each test.

Table 3. Comparison of the averaged shear strain increase from strain rosette measurement (SRM) and DIC analysis after each test (%).

specimen	test no.	1	2	3	4	5	6	7	8	9	10
A8	SRM	18.31	9.50	12.30	15.12	10.08	24.01	–	–	–	–
	DIC	13.65	6.25	10.84	9.37	8.13	n.a.	–	–	–	–
A19	SRM	n.a.	n.a.	4.50	4.03	4.93	4.53	n.a.	n.a.	10.4	15.6
	DIC	5.16	2.83	3.40	2.69	3.31	6.78	n.a.	7.13	29.6	n.a.
T1	SRM	8.51	5.45	5.76	8.20	4.65	n.a.	32.4	–	–	–
	DIC	2.14	5.16	4.14	7.37	3.76	1.81	n.a.	–	–	–

the polished surface. This roughness change reduced the reflected light and obscured the image. The grain boundaries in the middle showed void-like structures, whereas on the right and left sides, they still paralleled each other with a uniform shear strain.

(b) Ti6Al4V

Figure 6*a–h* shows stress–strain curves for Ti6Al4V, together with the correlated pictures of macro-deformation and DIC analysis results.

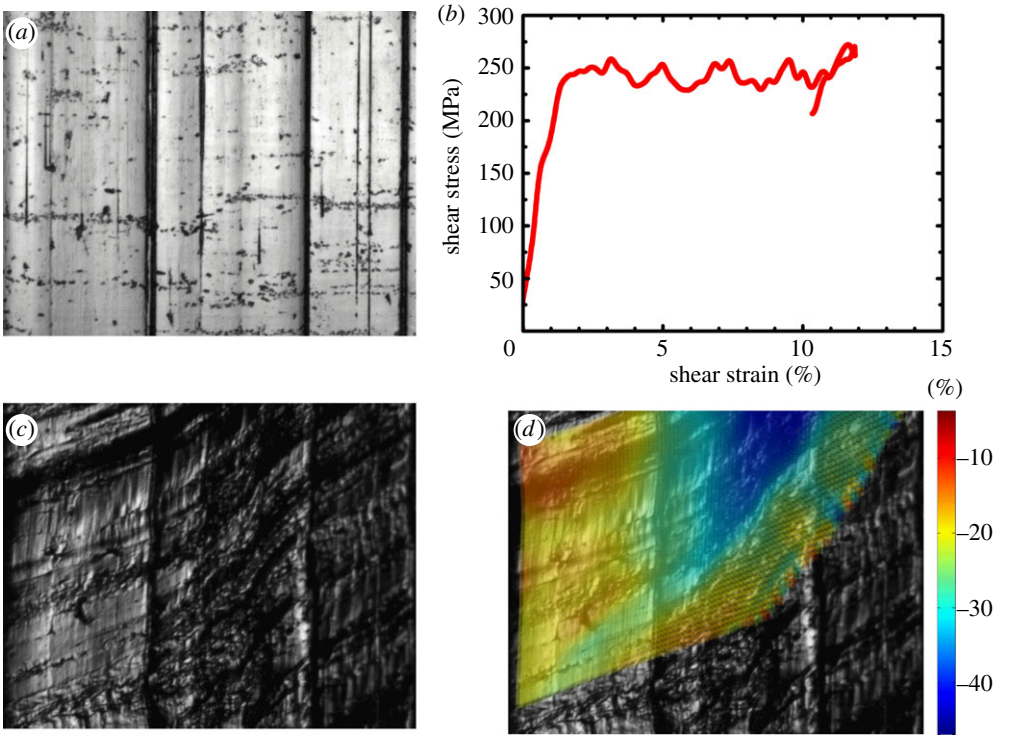

Figure 5. Strain and stress curves of the ninth loading and deformation localized in a band with 190 μm width in AA2024 specimen A19. The shattered grain boundaries on both sides paralleled each other. (*a*) Undeformed surfaces; (*b*) the strain and stress curve of the ninth loading; (*c*,*d*) deformed surface and shear strain distribution after the ninth loading.

The surface of the test range was polished and then etched away to observe the microstructure of Ti6Al4V. The phases could be observed under a microscope with 200–500 times magnification, and an objective lens was added to the camera system to achieve such magnification. There was marked contrast between the α phase (the dark one) and the β phase (the bright one), as shown in figure 6.

Ti6Al4V specimen T1 survived five rectangular torsional pulses and fractured on the sixth. The results were obtained by following the same procedure as that of the AA2024 sample. The shear strains from the strain gauge measurements, as well as those from DIC calculations, are shown in figure 6 and table 3.

4. Discussion

(a) Results of AA2024 and Ti6Al4V

Deformation localization was observed in the AA2024 specimen during loading according to the results in figures 4 and 5. It was notable that the shear strains from the strain rosette measurement and DIC analysis did not match at first loading, which may be owing to the clearance between all the specimens and bars. The results of shear strain increase from these two measurements are compared in table 3. The whole test region was captured for the A8 tests, and the averaged results from the strain gauge and DIC calculation were close. The discrepancies between the two sets of results for A19 were larger, as its DIC images were captured from a smaller region than that of A8. The strain increased faster in the strain localized region, as can be observed from the DIC results of strain in the central area of A8, as well as those of A19 after the ninth loading; the DIC results were higher than the total averaged strain from the strain gauge measurements.

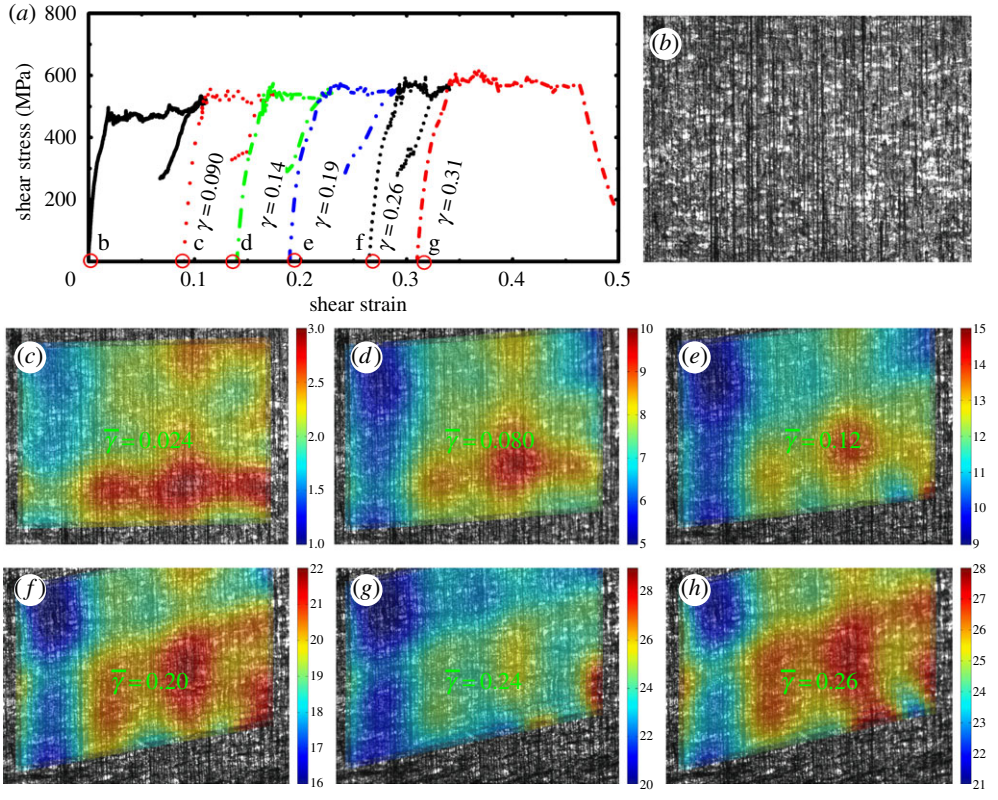

Figure 6. Strain–stress curves and the correlated microstructure evolution analysis of Ti6Al4V.

From the results of the Ti6Al4V specimen tested, shear localization was not found in the circular direction. The strain calculated from DIC and that obtained from strain rosette comparison are similar to those for AA2024.

The deformation of Ti6Al4V was much smaller than that of AA2024, even though the specimen was thinner (table 2) and the torsional load applied was larger (as shown in figure 3), which was as expected, because the yield strength of Ti6Al4V was much higher than that of AA2024.

The results for each material exhibited variations in dynamic response. The specimens with similar thickness and gauge length were under the same level of pulsed loading, although they fractured after different times of loading and in various manners. Some fractured along the circular direction, while some buckled under similar loading. The discrepancies in these 'identical' samples originated from the characteristic microstructure of each specimen. With the modification referred to in this paper, each stress–strain curve could be correlated to its microstructural evolution, thus the material properties could be extracted from the results for each specimen.

(b) Conclusion and summary

A modified SHTB system to observe the frozen microstructure and its evolution correlated with the stress–strain relationship was developed, and the principles, experimental set-up and procedure have been reported in this work. The preliminary results of the correlated study of two materials' τ–γ relation, shear localization and microstructure evolution in AA2024 have also been presented. By using the four-bar SHTB system, the reverberation of waves in the bars and the tested specimen can be considerably suppressed, thus the microstructure after a single torsional pulse loading can be preserved for static observation for shear localization and microstructure.

The results for each material showed variations in dynamic response: the specimens with similar thickness and gauge length fractured after different times of load, and in various manners of cracking and buckling. The characteristic microstructure of each specimen led to discrepancies in those 'identical' samples, thus the material properties had to be extracted from the statistical results of a lot of specimens. With the modification referred to in this paper, each stress–strain curve could be correlated to its own microstructure.

By interrupting tests on a given specimen, together with a fixed view-field *in situ* observation, the evolution of shear localization and microstructure correlated to stress–strain stage can be determined. Further experiments on the apparatus to reveal the mechanism of shear localization are made possible for future investigations.

Funding statement. The support from NSFC (grant nos. 11021262, and 11172305) is gratefully acknowledged.

References

1. Hopkinson B. 1914 A method of measuring the pressure produced in the detonation of high explosives or by the impact of bullets. *Phil. Trans. R. Soc. Lond. A* **213**, 437–456. (doi:10.1098/rsta.1914.0010)
2. Kolsky H. 1949 An investigation of the mechanical properties of materials at very high rates of loading. *Proc. Phys. Soc. B* **62**, 676. (doi:10.1088/0370-1301/62/11/302)
3. Baker WE, Yew CH. 1966 Strain-rate effects in the propagation of torsional plastic waves. *J. Appl. Mech.* **33**, 917–923. (doi:10.1115/1.3625202)
4. Duffy J, Campbell JD, Hawley RH. 1971 On the use of a torsional split Hopkinson bar to study rate effects in 1100–0 aluminum. *J. Appl. Mech.* **38**, 83–91. (doi:10.1115/1.3408771)
5. Field JE, Walley SM, Proud WG, Goldrein HT, Siviour CR. 2004 Review of experimental techniques for high rate deformation and shock studies. *Int. J. Impact Eng.* **30**, 725–775. (doi:10.1016/j.ijimpeng.2004.03.005)
6. Nemat-Nasser S, Isaacs JB, Starrett JE. 1991 Hopkinson techniques for dynamic recovery experiments. *Proc. R. Soc. Lond. A* **435**, 371–391. (doi:10.1098/rspa.1991.0150)
7. Xue Q, Shen LT, Bai YL. 1995 A modified split Hopkinson torsional bar in studying shear localization. *Meas. Sci. Technol.* **6**, 1557–1565. (doi:10.1088/0957-0233/6/11/002)
8. Xue Q, Shen LT, Bai YL. 1995 Elimination of loading reverberation in the split Hopkinson torsional bar. *Rev. Sci. Instrum.* **66**, 5298–5304. (doi:10.1063/1.1146102)
9. Bai YL, Xue Q, Xu YB, Shen LT. 1994 Characteristics and microstructure in the evolution of shear localization in Ti-6A1-4V alloy. *Mech. Mater.* **17**, 155–164. (doi:10.1016/0167-6636(94)90056-6)
10. Xu YB, Bai YL, Xue Q, Shen LT. 1996 Formation, microstructure and development of the localized shear deformation in low-carbon steels. *Acta Mater.* **44**, 1917–1926. (doi:10.1016/1359-6454(95)00306-1)
11. Xue Q, Cerreta E, Gray III G. 2007 Microstructural characteristics of post-shear localization in cold-rolled 316L stainless steel. *Acta Mater.* **55**, 691–704. (doi:10.1016/j.actamat.2006.09.001)
12. Bai YL. 1982 Thermo-plastic instability in simple shear. *J. Mech. Phys. Solids* **30**, 195–207. (doi:10.1016/0022-5096(82)90029-1)
13. Clifton RJ, Duffy J, Hartley KA, Shawki TG. 1984 On critical conditions for shear band formation at high strain rates. *Scr. Metall.* **18**, 443–448. (doi:10.1016/0036-9748(84)90418-6)
14. Wright TW, Batra RC. 1987 Adiabatic shear bands in simple and dipolar plastic materials. In *Macro- and micro-mechanics of high velocity deformation and fracture* (eds K Kawata, J Shioiri), pp. 179–188. Heidelberg, Germany: Springer.
15. Shawki TG, Clifton RJ. 1989 Shear band formation in thermal viscoplastic materials. *Mech. Mater.* **8**, 13–43. (doi:10.1016/0167-6636(89)90003-3)
16. Xing D, Bai YL, Cheng CM, Huang XL. 1991 On post-instability processes in adiabatic shear in hot rolled steel. *J. Mech. Phys. Solids* **39**, 1017–1042. (doi:10.1016/0022-5096(91)90050-X)
17. Backman ME, Finnegan SA, Shulz JC, Pringk JK. 1986 Scaling rules for adiabatic shear. In *Metallurgical applications of shock-wave and high-strain-rate phenomena* (eds LE Murr, KP Staudhammer, MA Meyers), pp. 675–687. New York, NY: CRC Press LLC.
18. Bai YL. 1989 Evolution of thermo-visco-plastic shearing. In *Proceedings of materials at high rates of strain* (ed. J Harding), pp. 99–110. Bristol, UK: Institute of Physics.

19. Anand L, Dillon O, Place TA, Vonturkovich BF. 1990 Report of the NSF workshop on localized plastic instabilities and failure criteria. *Int. J Plasticity* **6**, R1–R9. (doi:10.1016/0749-6419(90)90024-9)
20. Marchand A, Duffy J. 1988 An experimental study of the formation process of adiabatic shear bands in a structural steel. *J. Mech. Phys. Solids* **36**, 251–283. (doi:10.1016/0022-5096(88)90012-9)
21. Hartley KA, Duffy J, Hawley RH. 1987 Measurement of the temperature profile during shear band formation in steels deforming at high strain rates. *J. Mech. Phys. Solids* **35**, 283–301. (doi:10.1016/0022-5096(87)90009-3)
22. Giovanola JH. 1988 Adiabatic shear banding under pure shear loading. 1. Direct observation of strain localization and energy-dissipation measurements. *Mech. Mater.* **7**, 59–71. (doi:10.1016/0167-6636(88)90006-3)
23. Rittel D, Landau P, Venkert A. 2008 Dynamic recrystallization as a potential cause for adiabatic shear failure. *Phys. Rev. Lett.* **101**, 16550116. (doi:10.1103/PhysRevLett.101.165501)
24. Rittel D. 1999 On the conversion of plastic work to heat during high strain rate deformation of glassy polymers. *Mech. Mater.* **31**, 131–139. (doi:10.1016/S0167-6636(98)00063-5)
25. Rittel D, Wang ZG, Merzer M. 2006 Adiabatic shear failure and dynamic stored energy of cold work. *Phys. Rev. Lett.* **96**, 755027. (doi:10.1103/PhysRevLett.96.075502)